Propulsion hydrodynamics of a butterfly micro-swimmer

M. Iima[1] and A. S. Mikhailov[2]

[1] *Research Institute for Electronic Science, Hokkaido University, N20W10 Sapporo, 001-0020, Japan*
[2] *Department of Physical Chemistry, Fritz Haber Institute of the Max Planck Society, Faradayweg 4-6, 14195 Berlin, Germany*

PACS 47.61.-k – Micro- and nano- scale flow phenomena
PACS 47.15.G- – Low-Reynolds-number (creeping) flows
PACS 87.15.H- – Dynamics of biomolecules

Abstract. - Propulsion motion of a simple mechanical model at low Reynolds numbers is considered. The model consists of two spheroids (wings) connected by a hinge. Its non-reciprocal operation cycles represent combinations of flapping motions of the wings and of their rotations, resembling conformational motions characteristic for real protein machines and similar to the propulsion pattern of a butterfly. The net generated velocity and the net stall force, exhibited by an immobilized machine on its support, are calculated and their dependence on the model parameters is discussed.

Introduction. – It is well known that bacteria and other microorganisms can swim through fluids by periodically changing their shape. The only restriction, imposed by the laws of hydrodynamics at low Reynolds numbers, has been pointed out by Purcell [1] in the form of the "scallop theorem": a purely reciprocal cyclic motion, such as opening and closing of a scallop's shell, cannot generate net propulsion. General analysis of propulsion effects of an object cyclically changing its shape is available [2, 3].

Several theoretical models of propulsion have been considered to achieve non-reciprocal motion. The Purcell's three-link swimmer, a simplest model swimmer, consists of three rigid rods connected at two hinges each of which has one degree of freedom: the relative angle between two rods [1, 4–6]. The model with three linked spheres, presented by Najafi and Golestanian [7], has three spheres connected via two deformable rods(see also [8]). Examples of propulsion motion, characteristic for bacterial motions and involving cilia waves or rotation of flagella, have been considered [9–17].

Not only microorganisms, but even individual macromolecules operating as protein machines can cyclically change their shapes while being immersed into a fluid. Typically, a protein machine receives energy in the chemical form, with an ATP or other molecule binding to it as a ligand. This leads to a gradual change of the protein shape, representing a process of conformational relaxation of the protein-ligand complex to its equilibrium state . At some stage, the ligand is converted into a product (such as the ADP molecule) which then leaves the protein. After product detachment, the free protein molecule undergoes conformational relaxation back to its equilibrium state. Thus, the cycle of a machine consists of two relaxational motions, the forward one induced by ligand binding and the backward

one following product detachment. Generally, these two conformational motions do not follow the same trajectories in the conformational space (see, *e.g.*, [18]),which means that the motion is non-reciprocal. Therefore the swimming effect should be expected.

To obtain estimates of the magnitude of propulsion effects for molecular machines and to understand their dependence on the internal motions present, simple mechanical models can be used. While very rough estimates can be already gained by using the above-mentioned models of the elementary three-link or three-sphere swimmers(see, *e.g.*, [8]), it should be also noticed that the kinds of internal motions assumed in these two models are not quite typical for protein molecules. It is more often that a protein machine would possess only a single hinge connecting two relatively rigid parts. Nonetheless, the cyclic motion of a machine can still be non-reciprocal, because the shapes or the mutual orientation of the rigid blocks are not the same in the forward and back motions.

The simplest swimmer with single-hinge motions can be described as a *butterfly micro-swimmer*. Such butterfly has two wings connected via a hinge. Flapping motions of the wings are repeatedly performed. Inside each cycle, the forward and back flapping motions are not however completely reciprocal. Before the wings start to move back, they are rotated and therefore they get a different orientation with respect to the flapping direction. When the back flapping is completed, the wings are turned back and the initial configuration is restored, so that the next cycle starts with the same initial condition. For simplicity, the wings are modelled in our study as asymmertic spheroids (see Fig.1). The two spheroids are connected to the central node by two thin rigid rods which can perform hinge motions. Additionally, the spheroids can turn around the rods changing their orientation with respect to the induced flows.

Note that such movements indeed mimic the genuine butterfly's flapping motion in which the angle of attack in the downstroke differs from that in the upstroke [19]. However, real butterflies fly by generating macroscopic flows including dynamics of coherent vortices at relatively high Reynolds numbers where the effective viscosity is low. Owing to such effect, net propulsion can already be achieved by pure reciprocal motions (see [20, 21]). The butterfly micro-swimmer, considered in the present study, operates in the regime of low Reynolds numbers and of high effective viscocity, where the non-reciprocity of internal motions is a necessary condition for self-propulsion.

Directly solving the hydrodynamics equations at low Reynolds numbers, we determine the flows induced by the butterfly swimmer and the forces acting on it. This allows us to analytically estimate the net propulsion velocity of the swimmer, depending on the characteristic length sizes of the model and the parameters of the internal mechanical motions. We also calculate the stall force that should be applied to the swimmer to prevent its translational motions. Using these data, estimates for the parameter ranges characteristic for real protein machines are obtained.

Model. – We consider a simple butterfly model of a molecular machine consisting of two identical wings. Each wing represents a spheroid (Fig.1(b)) described by the equation

$$\frac{x^2+y^2}{a^2}+\frac{z^2}{a^2(1-\varepsilon)^2}=1. \tag{1}$$

It will be assumed that the spheroid is only slightly asymmetrical, so that $\varepsilon \ll 1$. The spheroids are attached to two rigid rods with length l which are connected at central hinge node O (Fig.1(c)). The rods are infinitely thin and have no direct effect on the fluid. They can move, changing their relative angle 2α. Additionally, spheroids can rotate around the rods. The angles β and γ between the symmerty directions of the two rods and the plane of hinge motions are changing as the result of such internal rotations. Only the symmetric case of $\gamma = -\beta$ will be considered below. The cyclic motion of this model consists of transitions $A \to B \to C \to D \to A$... between four distinct states A, B, C and D, each of which is characterized by a certain set of angles: A $[(\alpha,\beta)=(\alpha_0,0)]$, B $[(\alpha,\beta)=(\alpha_1,0)]$,

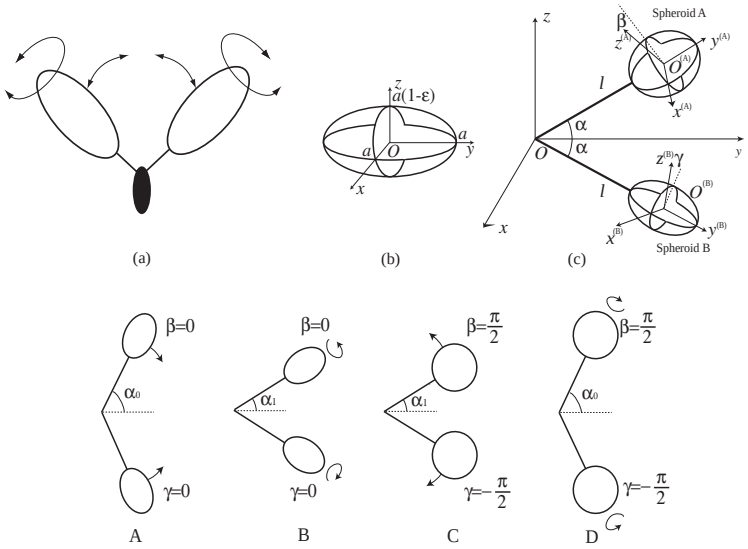

Fig. 1: (a) The butterfly micro-swimmer. Propulsion is generated by a combination of the flapping motion and of rotations. Coordinates are defined for a single spheroid [(b)] and for the model of two spheroids connected though a hinge [(c)]. The cyclic motion of the model represents sequential transitions between the states A, B, C and D.

C $[(\alpha,\beta)=(\alpha_1,\frac{\pi}{2})]$, and D $[(\alpha,\beta)=(\alpha_0,\frac{\pi}{2})]$ (see Fig.1,bottom). After the state D, the model returns to the state A. To perform analytical calculaton, we assume that the distance between two spheroids, $2l\sin\alpha$, is sufficiently larger than the length scale of the spheroid, $2a$; *i.e.*, $a \ll l\sin\alpha$. Under this assumption, the flow caused by the motion of a wing can be assumed uniform at the position of the other wing.

The dimensionless parameters specifying the model geometry are: ε, expressing the asymmetry of the spheroid ($\varepsilon=0$ corresponds to a sphere), and $\zeta=a/l$, the length ratio of the longer axis of the spheroid and the rod. We assume that $\varepsilon \ll 1$ and $\zeta \ll \sin\alpha$.

The flow around the model is assumed to be governed by the Stokes equations, *i.e.*, $\mu\Delta\boldsymbol{u}=\nabla p,\ \nabla\cdot\boldsymbol{u}=0$, where $\mu,\boldsymbol{u},p$ are the viscosity, the flow field, and the pressure, respectively. In this case, the flow induced by a spheroid moving with translational velocity $\boldsymbol{v}$ and rotating with angular velocity $\boldsymbol{\omega}$ is given by $\boldsymbol{u}=\boldsymbol{u}^{\rm trans.}+\boldsymbol{u}^{\rm rot.}$, where the components of $\boldsymbol{u}^{\rm trans.}$ and $\boldsymbol{u}^{\rm rot.}$ can be calculated by a perturbation method, described in Ref. [22]. The calculations yield $u_i^{\rm trans.}=C_{ij}v_j, u_i^{\rm rot.}=D_{ij}\omega_j$ (Einstein's summation rule is applied throughout the paper), where

$$C_{ij}(\boldsymbol{r}) = \frac{1}{4}(3\eta+\eta^3-3\varepsilon p)\delta_{ij}+\frac{3}{4}(\eta-\eta^3+\varepsilon p)\frac{r_ir_j}{r^2}, \quad (2)$$

$$D_{ij}(\boldsymbol{r}) = (1-\frac{6}{5}\varepsilon)\eta^3\varepsilon_{ijk}r_k. \quad (3)$$

Here $p\equiv\cos(2\theta)+1, \eta\equiv a/r, \boldsymbol{r}=(x,y,z)\equiv(r_1,r_2,r_3)$ is the position vector, and ε_{ijk} is the Eddinton's epsilon ($\varepsilon_{ijk}=1$ for all combinations of indexes i,j and k obtained by a cyclic permutation from (1,2,3) and $\varepsilon_{ijk}=-1$ otherwise). Note that we have kept all terms up to $O(\eta^3\varepsilon)$ in the above perturbation expansions. The force acting on the spheroid moving with velocity $\boldsymbol{v}$ and angular velocity $\boldsymbol{\omega}$, $\boldsymbol{F}$, is given by $F_i=-6\pi\mu aK_{ij}v_j$, where $K_{ij}=\delta_{ij}-\varepsilon k_{ij}$ with $k_{ij}\equiv\frac{2}{5}\delta_{ij}$ for $i=1,2$ and $k_{ij}\equiv\frac{1}{5}\delta_{ij}$ for $i=3$.

Below, three coordinate systems shall be used (Fig.1(b)). The first of them has the origin of coordinates in the hinge center O, with the (y,z) plane corresponding to the hinge motion. The two others have their origins in the centers of the spheroids A and B,

respectively. Their z-axes correspond to the axes of the symmetry. Suppose that $\boldsymbol{a}^{(O)}$, $\boldsymbol{a}^{(A)}$ and $\boldsymbol{a}^{(B)}$ are representations of the same vector in the three coordinate systems. Then, they are related via a transformation $\boldsymbol{a}^{(A)} = T^{AO}\boldsymbol{a}^{(O)}$ and a similar equation for $\boldsymbol{a}^{(B)}$. The transformation matrices can be expressed through the rotation matirices $R_i(\theta)$ (rotation by angle θ around the r_i-axis) as $T^{AO} = R_y(-\beta)R_x(-\alpha), T^{BO} = R_y(-\gamma)R_x(\alpha)$. Note that $T^{OA} = (T^{AO})^{-1}$ and $T^{OB} = (T^{BO})^{-1}$. Hereafter, the superscript (O) will be omitted for simplicity.

Using these notations, forces acting on the model can be determined. Let us define the velocity of the center of mass of the model as $\boldsymbol{U}$, the relative velocity of the spheroid A to the center of mass of the model as $\boldsymbol{v}_A$, and that of the spheroid B as $\boldsymbol{v}_B$. Then, the forces acting on the spheroids A and B, $\boldsymbol{F}_A$ and $\boldsymbol{F}_B$ are given by

$$\boldsymbol{F}_A^{(A)} = -6\pi\mu aK(\boldsymbol{v}_A^{(A)} - \boldsymbol{u}_B^{(A)}(\boldsymbol{r}_A - \boldsymbol{r}_B) + \boldsymbol{U}^{(A)}), \tag{4}$$

$$\boldsymbol{F}_B^{(B)} = -6\pi\mu aK(\boldsymbol{v}_B^{(B)} - \boldsymbol{u}_A^{(B)}(\boldsymbol{r}_B - \boldsymbol{r}_A) + \boldsymbol{U}^{(B)}), \tag{5}$$

where $\boldsymbol{u}_B^{(A)}(\boldsymbol{r}_A - \boldsymbol{r}_B)$ is the velocity induced at $\boldsymbol{r} = \boldsymbol{r}_A$ due to the motion of the spheroid B at $\boldsymbol{r} = \boldsymbol{r}_B$ and *vice versa*:

$$\boldsymbol{u}_B^{(A)}(\boldsymbol{r}_A - \boldsymbol{r}_B) = T^{AB}\boldsymbol{u}_B^{(B)} \tag{6}$$

$$= T^{AB}(C^{(B)}\boldsymbol{v}_B^{(B)} + D^{(B)}\boldsymbol{\omega}_B^{(B)}), \tag{7}$$

$$\boldsymbol{u}_A^{(B)}(\boldsymbol{r}_B - \boldsymbol{r}_A) = T^{BA}\boldsymbol{u}_A^{(A)} \tag{8}$$

$$= T^{BA}(C^{(A)}\boldsymbol{v}_A^{(A)} + D^{(A)}\boldsymbol{\omega}_A^{(A)}), \tag{9}$$

The force-balance equation is:

$$\boldsymbol{F}_{\rm ex} + \boldsymbol{F}_A + \boldsymbol{F}_B = \boldsymbol{0}, \tag{10}$$

where we have assumed that an external force $\boldsymbol{F}_{\rm ex}$ acts at the hinge. By using eq.(10), we analyze further two characteristic cases: free-swimming with $\boldsymbol{F}_{\rm ex} = 0$ and the stall condition, where the hinge is fixed at some point.

Free swimming. – For the free-swimming case, we are interested in the swimming velocity $\boldsymbol{U}$ under no external force: $\boldsymbol{F}_{\rm ex} = \boldsymbol{0}$.

For the $A \to B$ and $C \to D$ motions, $\mathrm{d}\beta/\mathrm{d}t = 0$. Because of the symmetry of these internal motions, we have $U_x = U_z = 0$. A straightforward calculation based on eq.(10) yields the velocity U_y and the displacement $\Delta y(\alpha_a, \alpha_b; \beta)$ along the y direction within the time interval $[t_a, t_b](\alpha = \alpha_a$ at $t = t_a$ and $\alpha = \alpha_b$ at $t = t_b)$ as

$$U_y = f(\alpha, \beta)l\frac{\mathrm{d}\alpha}{\mathrm{d}t}, \tag{11}$$

$$\Delta y(\alpha_a, \alpha_b; \beta) = l\int_{\alpha_a}^{\alpha_b} f(\alpha, \beta)\mathrm{d}\alpha. \tag{12}$$

The explicit forms of $f(\alpha, \beta)$ for $\beta = 0$ and $\beta = \pi/2$ are given by:

$$f(\alpha, \beta) = f_0(\alpha, \beta) + \varepsilon f_1(\alpha, \beta), \tag{13}$$

where $f_0(\alpha, 0) = f_0(\alpha, \pi/2) = \sin\alpha, f_1(\alpha, 0) = (17/10)\cos^2\alpha\sin\alpha, f_1(\alpha, \pi/2) = 0$ up to their leading orders.

For the $B \to C$ and $D \to A$ motions, $\mathrm{d}\alpha/\mathrm{d}t = 0$. In this case, the symmetry impies $U_y = U_z = 0$. The velocity U_x and the displacement $\Delta x(\alpha; \beta_a, \beta_b)$ in the x direction within the time interval $[t_a, t_b](\beta = \beta_a$ at $t = t_a$ and $\beta = \beta_b$ at $t = t_b)$ are:

$$U_x = g(\alpha)\zeta^3 l\frac{\mathrm{d}\beta}{\mathrm{d}t}, \tag{14}$$

$$\Delta x(\alpha; \beta_a, \beta_b) = \zeta^3 l\int_{\beta_a}^{\beta_b} g(\alpha)\mathrm{d}\beta = \zeta^3 l(\beta_b - \beta_a)g(\alpha), \tag{15}$$

where $g(\alpha) = -(1/20)(5-6\varepsilon)\cos\alpha/\sin^2\alpha$.

The total vector displacement within one cycle, $\Delta\boldsymbol{X} = (\Delta X, \Delta Y, \Delta Z)$, is:

$$\Delta X = \frac{\pi}{2}\zeta^3 l(g(\alpha_1) - g(\alpha_0)), \tag{16}$$

$$\Delta Y = -\varepsilon l \int_{\alpha_1}^{\alpha_0} f_1(\alpha, 0)\mathrm{d}\alpha, \tag{17}$$

$$\Delta Z = 0. \tag{18}$$

The net propulsion velocity is $\langle \mathbf{V} \rangle = \Delta\mathbf{X}/T$ where T is the cycle time.

The stall condition. – Now we assume that the translational motion of the model is prevented by fixing at its hinge center O, but the model can still freely rotate around this center. Because of the symmetry of the model, the induced rotation takes place along the $z-$axis (Fig.1(c)) and is characterized by some angular velocity Ω_z. Due to the rotation, the orientation of the stall force, needed to prevent translational motion, is also changing with time. If the angular velocity is constant, the stall force is always directed towards the hinge center. In the coordinate frame attached to the model (Fig.1(c)) it has only the component along the $y-$direction, i.e. $\mathbf{F}_{\rm ex} = (0, F_{\rm stall}, 0)$. Note that, because of the rotation, the wings have instantaneous linear velocities $U_x = \Omega_z l\cos\alpha$ along the $x-$axis in this frame.

In the $A \to B$ and $C \to D$ transitions, $\mathrm{d}\beta/\mathrm{d}t = 0$ and therefore $\Omega_z = 0$ due to the symmetry. A straightforward calculation yields the instantaneous stall force $F_{\rm stall}$ and the total momentum transfer $I(\alpha_a, \alpha_b; \beta)$ along the $y-$direction within the time interval $[t_a, t_b]$,

$$F_{\rm stall} = h(\alpha, \beta)\mu l^2 \zeta \frac{\mathrm{d}\alpha}{\mathrm{d}t}, \tag{19}$$

$$I(\alpha_a, \alpha_b; \beta) = \mu l^2 \zeta \int_{\alpha_a}^{\alpha_b} h(\alpha, \beta)\mathrm{d}\alpha. \tag{20}$$

The explicit forms for $h(\alpha, \beta)$ for $\beta = 0, \pi/2$ are

$$h(\alpha, \beta) = h_0(\alpha, \beta) + \varepsilon h_1(\alpha, \beta), \tag{21}$$

where $h_0(\alpha, 0) = h_0(\alpha, \pi/2) = -12\pi\sin\alpha, h_1(\alpha, 0) = -(3\pi/10)(7\sin\alpha + 15\sin(3\alpha)), h_1(\alpha, \pi/2) = (24\pi/5)\sin\alpha$ up to their leading orders.

In the $B \to C$ and $D \to A$ transitions, $\mathrm{d}\alpha/\mathrm{d}t = 0$ and rotation along the $z-$axis takes place. The instantaneous angular velocity Ω_z and the total angle increment $\Delta\Theta(\alpha; \beta_a, \beta_b)$ are caclulated as

$$\Omega_z = \theta(\alpha)\zeta^3 \frac{\mathrm{d}\beta}{\mathrm{d}t}, \tag{22}$$

$$\Delta\Theta = \theta(\alpha)\zeta^3(\beta_b - \beta_a), \tag{23}$$

where $\theta(\alpha) = -g(\alpha)/\cos\alpha = (1/20)(5-6\varepsilon)/\sin^2\alpha$. Note that, to prevent translational motion during these transitions, some stall force acting along the $y-$direction should be applied. This force is equal to the sum of the the centrifugal forces of the two wings, $f = 2m\Omega_z^2 l\cos\alpha$ where m is the mass of a wing. As we show in the Discussion section, such centrifugal forces are however very small on the microscales and can be neglected, as compared with the stall forces needed in two other transitions.

In each machine cycle, the total momentum transfer $I_{\rm total}$, the total angle increment $\Delta\Theta_{\rm total}$ and the net stall force $\langle F_{\rm stall} \rangle$, averaged over the cycle, are

$$I_{\rm total} = \mu l^2 \zeta\varepsilon \int_{\alpha_1}^{\alpha_0} (h_1(\alpha, \frac{\pi}{2}) - h_1(\alpha, 0))\mathrm{d}\alpha, \tag{24}$$

$$\Delta\Theta_{\rm total} = \frac{\pi}{2}\zeta^3 \left\{\theta(\alpha_1) - \theta(\alpha_0)\right\}, \tag{25}$$

$$\langle F_{\rm stall} \rangle = \frac{I_{\rm total}}{T}. \tag{26}$$

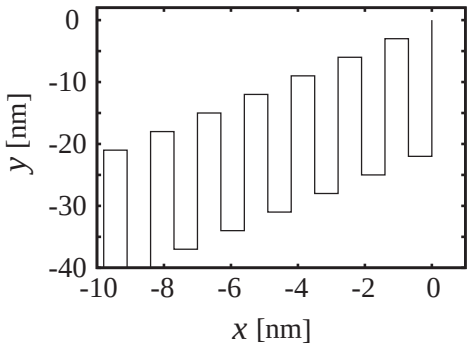

Fig. 2: Locomotion path of the model.

The net angular velocity is $\langle \Omega_z \rangle = \Delta\Theta_{\rm total}/T$. Note that the angle increment $\Delta\Theta_{\rm total}$ is proportional to ζ^3 and therefore is small; after each cycle, the model only slightly changes its spatial orientation.

Discussion. – In this section we analyze our analytical results both for the free-swimming and the stall cases and provide estimates for the magnitude of the propulsion velocity and the stall force.

Our analytical derivations have been performed assuming that the spheroid is only slightly asymmetric ($\varepsilon \ll 1$) and that the distance between two spheroids is much shorter than the spheroid radius ($\zeta \ll \sin\alpha$). The strongest propulsion effects are reached, as intuitively expected, for the largest magnitude of the hinge motion, which corresponds to $\alpha_1 \to 0$ and $\alpha_0 \to \pi$. In this limit, analytical expressions get simplified. The net relative displacements along $x-$ and $y-$directions per single cycle are $\Delta X/l \approx -(\pi\zeta^3/8)(1/\alpha_1^2 + 1/(\pi-\alpha_0)^2)$ and $\Delta Y/l \approx -(17/15)\varepsilon$. The smallest possible hinge angle α_1 is constrained by the condition that spheroids still do not touch each other in the final state, *i.e.* $\sin\alpha_1 > \zeta$. Thus, the smallest possible angle is of the order $\alpha_1 = \zeta$. Similar arguments show that the largest possible hinge angle should satisfy $\pi - \alpha_0 = \zeta$ by the order of magnitude. Therefore, the maximum net propulsion velocities along the $x-$ and $y-$directions can be roughly estimated as $\langle V_x \rangle \approx -(\pi/4)\zeta(l/T)$ and $\langle V_y \rangle \approx -(17/15)\varepsilon(l/T)$ where T is the duration of a single machine cycle.

Note that propulsion velocity $\langle V_x \rangle$ does not vanish when $\varepsilon = 0$, *i.e.* for the limit when spheroids become spheres. Even in this case, sphere rotations, corresponding to transitions $B \to C$ and $D \to A$ in the model, induce hydrodynamical flows in the surrounding fluid and the cycle is non-reciprocal. On the other hand, $\langle V_y \rangle = 0$ because the opening motion is then symmetric to the closing motion with respect to the $x-y$ plane. Generally, $\langle V_x \rangle \propto \zeta$ and $\langle V_y \rangle \propto \varepsilon$ for the maximal propulsion velocities that can be reached.

The maximum stall force (needed to prevent translational motion of the machine) is given by eq. (26). Examining this equation, we find that the maximal stall force is again required when $\alpha_1 \to 0$ and $\alpha_0 \to \pi$.Similar discussion to the free-swimming case leads to the estimation of the stall force as $\langle F_{\rm stall} \rangle \approx (84/5)\pi\varepsilon\zeta(\mu l^2/T)$ where μ is the fluid viscosity. It is proportional to both small parameters ε and ζ.

Finally, we can also estimate the maximum angular velocity $\langle \Omega_z \rangle$ of the machine pinned at its hinge center. It should be remarked that $\langle \Omega_z \rangle$ vanishes when the maximum propulsion efficiency is achieved, although it does not vanish in general. When the largest hinge angle is $\alpha_0 = \pi/2$, we obtain $\langle \Omega_z \rangle \approx (\pi/8)\zeta(1/T)$. This angular velocity does not depend on the small parameter ε.

In numerical estimates, we choose the following parameters for the geometry of our model: $l = 10$nm, $a = 3$nm, $\varepsilon = 1/3$, $\alpha_0 = \pi - 3/10$, $\alpha_1 = 3/10$, $\mu = 10^{-3}$Pa·s, and

$T = 1$ms. Their orders are those of a typical molecular machine. We note that these values give $\varepsilon = 1/3$ and $\zeta = 3/10$. The value of α_1 satisfies $\alpha_1 = \zeta$, which corresponds to the maximum propulsion efficiency.

For the free-swimming case, these parameters give the increments during each cycle as follows: $\Delta y_{A\to B} = -22\text{nm}, \Delta x_{B\to C} = -0.70\text{nm}, \Delta y_{C\to D} = 19\text{nm}, \Delta x_{D\to A} = -0.70\text{nm}$, and other components are zero. Consequently, the mean velocity is: $\boldsymbol{V}_{\text{mean}} = (-1.4, -3.3)[\text{nm/ms}]$. The path of the model is staggered, as shown in Fig.2. We note that the path is helical when $\alpha_0 < \pi/2$. For the stall condition, the momentum and angle increment during each process are given as follows: $I_{A\to B} = 2.3 \times 10^{-3}\text{pN}\cdot\text{ms}, I_{C\to D} = -1.9 \times 10^{-3}\text{pN}\cdot\text{ms}, \Theta_{B\to C} = -\Theta_{D\to A} = 0.012 \times 2\pi$, and other components are zero. The net stall force is: $\langle F_{\text{stall}}\rangle = \frac{I_{A\to B}+I_{C\to D}}{T} = 4.7 \times 10^{-4}\text{pN}$. The centrifugal forces f during the transitions $B \to C$ and $D \to A$ motions are of the order of 10^{-25}pN if $l \sim 10\text{nm}, \Omega_z \sim 10^{-4}\text{rad/s}, m \sim 10^3\text{kDa} \simeq 10^{-21}\text{kg}$ with $f = 2ml\Omega_z^2$ where m is the inertia mass of the wing. Therefore, they can indeed be neglected when the net stall force, averaged over a cycle, is calculated. Note that, because of the approximations used, the above numerical estimates should be viewed as providing only the order-of-magnitude evaluations of the respective effects.

Conclusions. – The butterfly micro-swimmer can propel itself and, when translationally immobilized, it exhibits some force on its support. Our analysis has been performed assuming the existence of two small parameters ε and ζ, specifying the asymmetry of spheroids (wings) and their relative sizes as compared to the length of the connecting rods. The maximum propulsion is realized when the utmost flapping angles α_1 and α_0 are close to 0 and π. Then, the net translational increments per one cycle are esimated as $(\Delta X/l, \Delta Y/l, \Delta Z/l) = (O(\zeta), O(\varepsilon), 0)$. Generally, if the flapping angles are not close to 0 and π, the estimates $(\Delta X/l, \Delta Y/l, \Delta Z/l) = (O(\zeta^3), O(\varepsilon), 0)$. The net stall force, averaged per a cycle, is of the order of $\langle F_{\text{stall}}\rangle / (\mu l^2/T) = O(\zeta\varepsilon)$ in both cases.

The considered model of the butterfly swimmer has internal mechanical motions which are similar to the hinge motions typical for protein machines. Obviously, it cannot be viewed as a realistic model for proteins - the latter never have regular geometrical shapes bounded by smooth surfaces. Moreover, hydrodynamic fluctuations become important on the nanoscales, but they have been neglected in our study. Nonetheless, in absence of more realistic descriptions, our results can be used to get rough estimates of propulsion effects for molecular machines. For a machine of linear size of 10 nm and the cycle time of 1 ms, we obtain, as the upper estimates, the propulsion velocities of the order of 1 μm/s and the propulsion (stall) forces of the order of 10^{-4} pN. For comparison, the characteristic force generated by a protein motor, moving along a filament and transporting a cargo, is about 1 pN. Moreover, due to thermal Brownian motion a molecule will move on the average over the distance of a micrometer in one millisecond, as compared with the distance of about 1 nanometer per millisecond due to hydrodynamical self-propulsion. We see that propulsion effects for individual molecular machines as nano-swimmers are very weak. However, hydrodynamical propulsion forces can nonetheless be essential for the collective behavior of large populations of molecular machines. Recently, properties of thin liquid films with floating molecular machiens have been considered and it was found that even the machiens generating propulsion forces of down to 10^{-5} pN can induce instabilities of the film surface and development of active hydrodynamical flows [23].

Thus, we have proposed a new model of a micro-swimmer and obtained analytical and numerical estimates for the propulsion properties of this model.

* * *

REFERENCES

[1] Purcell E. M., *Am. J. Phys.* , **45** (1977) 3.
[2] Shapere A. and Wilczek F., *Phys. Rev. Lett.* , **58** (1987) 2051.
[3] Avron J. E. and Raz O., *New J. Phys.* , **10** (2008) 063016.
[4] Becker L. E., Koehler S. A. and Stone H. A., *J. Fluid. Mech.* , **490** (2003) 15.
[5] Tam D. and Hosoi A. E., *Phys. Rev. Lett.* , **98** (2007) 068105.
[6] Kay E. R., Leigh D. A. and Zerbetto F., *Angew. Chem. Int. Ed.* , **46** (2007) 72.
[7] Najafi A. and Golestanian R., *Phys. Rev. E* , **69** (2004) 062901.
[8] Golestanian R. and Ajdari A., *Phys. Rev. Lett.* , **100** (2008) 038101.
[9] Taylor G. I., *Proc. Proc. R. Soc. Lond. A.* , **209** (1951) 447.
[10] Brennen C., *J. Fluid. Mech.* , **65** (1974) 799.
[11] Blake J. R., *J. Fluid. Mech.* , **46** (1971) 199.
[12] Blake J. R., *J. Fluid. Mech.* , **49** (1971) 209.
[13] Ehlers K. M., Samuel A. D. T., Berg H. C. and Montgomery R., *Proc. Natl. Acad. Sci.* , **93** (1996) 8340.
[14] Lauga E., *Phys. Rev. E* , **75** (2007) 041916.
[15] Felderhof B. U., *Phys. Fluilds* , **18** (2006) 063101.
[16] Qian B., Powers T. R. and Breuer K. S., *Phys. Rev. Lett.* , **100** (2008) 078101.
[17] Rapaport D. C., *Phys. Rev. Lett.* , **99** (2007) 238101.
[18] Togashi Y. and Mikhailov A. S., *Proc. Natl. Acad. Sci.* , **104** (2007) 8697.
[19] Ellington C. P., *Phil. Trans. R. Soc. Lond. B* , **305** (1984) 1.
[20] Iima M. and Yanagita T., *J. Phys. Soc. Japan* , **70** (2001) 5.
[21] Childress S. and Dudley R., *J. Fluid Mech.* , **498** (2004) 257.
[22] Happel J. and Brenner H., *Low Reynolds Number Hydrodynamics with special applications to particular media* (Martinus Nijhoff Publishers, The Hague) 1983.
[23] Alonso S. and Mikhailov A. S., *preprint arXiv:0810.1595v1[nlin.PS]* , (2008) .